

# Use of Landsat 7 ETM<sup>+</sup> Data for the Geological Structure Interpretation: Case Study of the Ngoura-Colomines Area, Eastern Cameroon

Jonas Didero TAKODJOU WAMBO<sup>1</sup>, Sylvestre GANNO<sup>1,\*</sup>, Aloysius AFAHNWIE NGAMBU<sup>2</sup>, Emmanuel NOMO NEGUE<sup>1</sup>, Joseph MVONDO ONDOA<sup>1</sup>, Jean Paul NZENTI<sup>1</sup>

<sup>1</sup>Department of Earth Sciences, University of Yaoundé I, P. O. Box 812 Yaounde, Cameroon

<sup>2</sup>Department of Geology, University of Buea, P. O. Box 63 Buea, Cameroon

\*Corresponding author: [sganno@uy1.uninet.cm](mailto:sganno@uy1.uninet.cm)

**Abstract** Remote sensing and Geographical Information System (GIS) technology have opened a new era in the field of applied geology. In this study, combined field and remote sensing applications through the processing of the Landsat-7 Enhance Thematic Mapper Plus (ETM<sup>+</sup>) were used to monitor to geologic structures in Ngoura-Colomines area. This mapping approach led to the detection of 654 lineaments in which two main types have been distinguished. The type-I (15%) shows two main directions (NE-SW and NW-SE) and corresponds to large-scale or regional structures while type-II (85%) with dominant NE-SW-trends represents foliation trajectories. In addition, type-I lineaments are compatible with the Riedel fault system composed of P and P' fractures oriented NE-SW and NNE-SSW respectively; E-W trending R fractures and R' fractures with NW-SE trends. Our findings provide the evidence of a polyphase ductile-brittle structures such as shear zone and faults. These structures constitute pathway for both mineralizing fluids and ground water circulation. Since several gold artisanal mines exist in Ngoura-Colomines area, the proposed mapping approach is an important guide for the identification of the structures that control the gold mineralisation in the area.

**Keywords:** Landsat ETM<sup>+</sup> images, Lineaments, Riedel fault system, Ngoura-colomines

**Cite This Article:** Takodjou Wambo, J.D., Ganno, S., Afahnwie, N.A., Nomo, N.E., Mvondo, O.J., and Nzenti, J.P., "Use of Landsat 7 ETM<sup>+</sup> Data for the Geological Structure Interpretation: Case Study of the Ngoura-Colomines Area, Eastern Cameroon." *Journal of Geosciences and Geomatics*, vol. 4, no. 3 (2016): 61-72. doi: 10.12691/jgg-4-3-3.

## 1. Introduction

Remote Sensing and Geographical Information System technology play a major role in thematic map generation and integrated analysis for mapping, managing and monitoring the natural resources. A remote sensing observation from space provides a synoptic view of terrain, thus provide ability in detecting lithology, land form and lineaments on the imagery. Since more than two decades, satellite imagery has been used for the identification and mapping of geologic structures which appear in geomorphology [1,2]. Lineaments are the linear, rectilinear and curvilinear features of tectonic origin observed on satellite image. These lineaments normally show tonal, textural, soil tonal, relief, drainage and vegetation linearity's and curvilinearities on satellite data. The identification of these structures and specifically of linear structures or lineaments can be successfully done by visual interpretation of aerial photographs, but nowadays, with the development of SIG technology, the automatic processing of satellite images such as SRTM and Landsat ETM images is highly recommended because of the high resolution of such data and the quantity of the information that they can provided. Many authors (eg., [3,4] and

references therein) have suggested that the combination of SIG techniques and field mapping is the more efficiency tools for geological map in rainforest areas. In a remote sensing study, interpretation of the lineament constitutes the essential key for geological and structural mapping [5]. Once the framework of lineaments has been set-up, the interpretation and validation of these structures are based on their comparison with field data. This exercise is complex in humid tropical region due to the important vegetation cover and the thick terrigenous materials recovery, which lead to the scarcity of outcrops [6,7], or of the discontinuity of outcrops when they exist [3]. The principle of the analysis of lineaments is that the principal collectors of the drainage systems as well as the resulting reliefs are dependent on the surrounding structures and thus carry a mark of the surrounding tectonics [7,8,9]. In the satellite images, all the linear features do not automatically correspond to geologic structures. For example, roads, railway and electrical lines as well as other human infrastructures are seen as lineaments. The challenge of the study of lineaments detection is to discriminate these objects and giving their geologic significance. Akame et al. [10] have suggested that the extraction of lineaments without applying directional filters does not bring out all the lineament networks, but it

remains an important step in the pre-analysis of structural mapping.

In characterizing the tectonic framework of the Ngoura-Colomines area, the present study also improves the knowledge on the geologic structures of the Pan African basement of the eastern Cameroon. Major and minor lineaments were interpreted from the satellite data and validated with the field studies. The approach used as well as the obtained data constitute an important guide for the mineral exploration in the area, since many artisanal gold mines exist in the Ngoura-Colomines.

## 2. Geologic Setting

Ngoura-Colomines area is located to the eastern Cameroon and extends between latitudes  $4^{\circ} 50' 02''$  and  $5^{\circ} 03' 33''$  N and longitudes  $14^{\circ} 08' 23''$  and  $14^{\circ} 25' 02''$  E (Figure 1). The geomorphology of the area falls within the so called ‘Southern Cameroonian plateau’, characterized by elevations that range between 550 and 850 m. The general topography of the area consists of small hills generally resulting from erosion which, in most cases, ends in valleys (Figure 1).

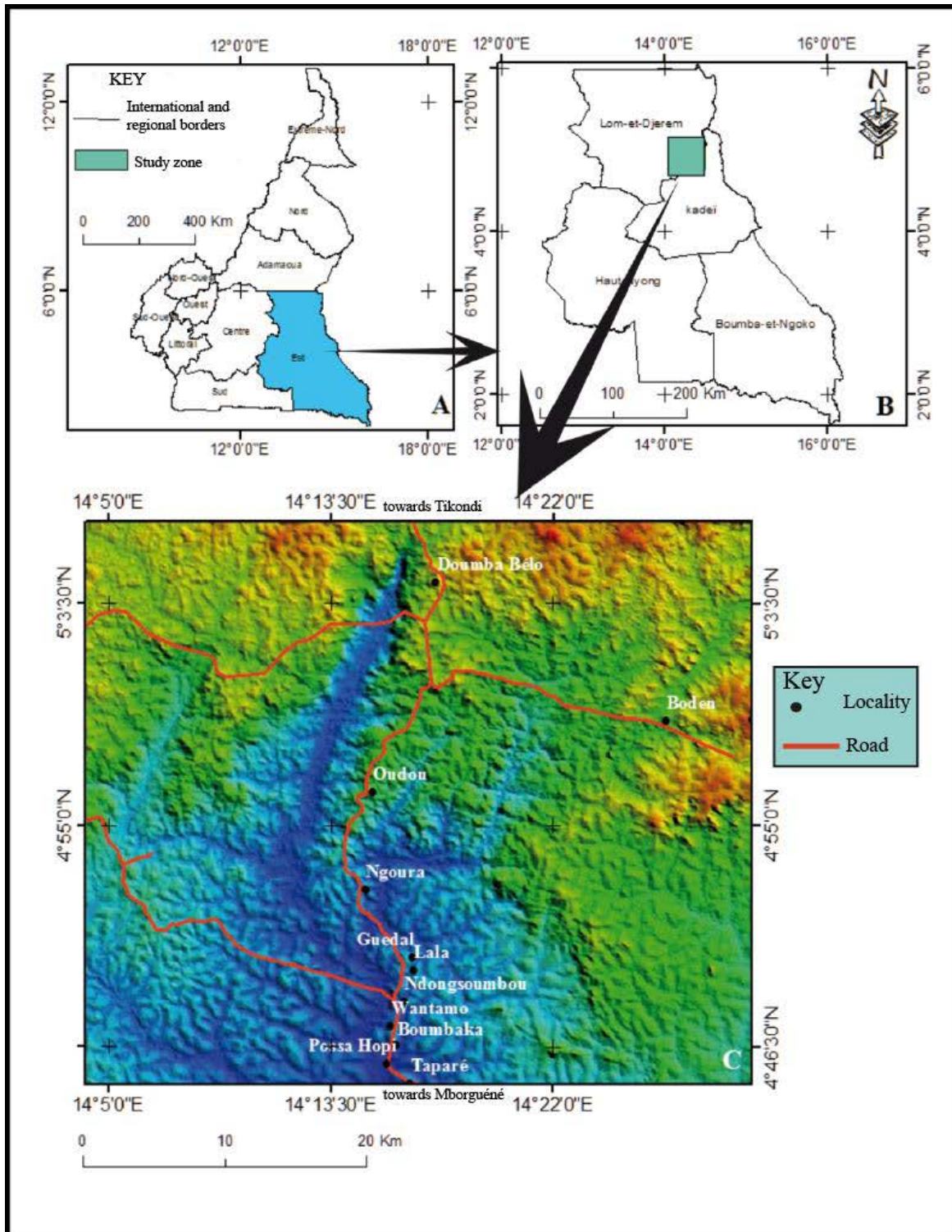


**Figure 1.** Location of area of study: A) Administrative map of Cameroon; B) Administrative map of the eastern region of Cameroon; C) Digital elevation model of the study area

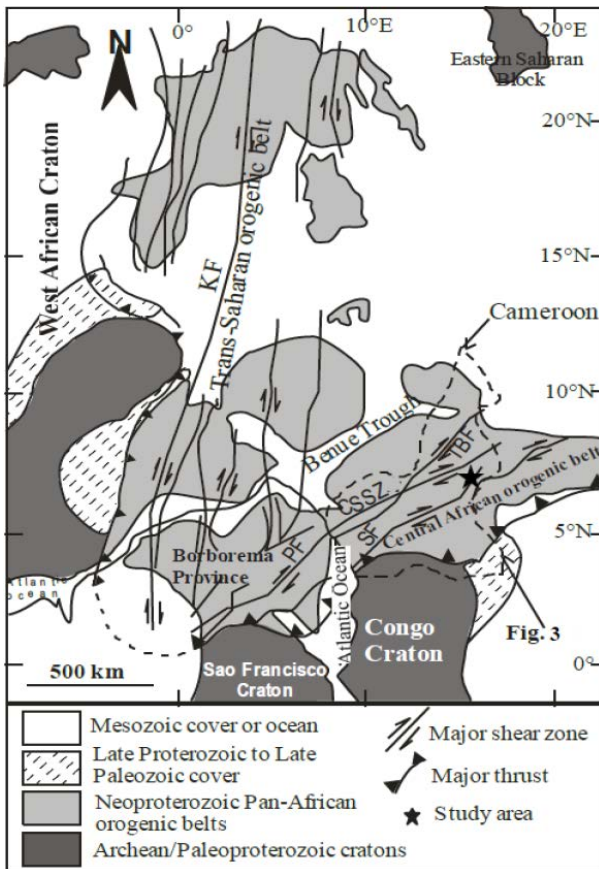


**Figure 2.** Pre-drift reconstruction of Pan-African and Brasiliano terranes (modified from [19]): CCSZ: Central Cameroon Shear Zone; SF: Sanaga Fault; TF: Tibati Fault; PF: Patos Fault

The study area belongs to the North-Equatorial Fold Belt (NEFB) or Central African Orogen which is a major Neoproterozoic Orogen linked to the Trans-Saharan belt of western Africa and to the Brazilian Orogen of northeastern Brazil (Figure 2). In Cameroon, the Neoproterozoic realm [11-16] is subdivided into three geodynamic domains from south to north (Figure 3): (1) the southern domain, which corresponds to the northern edge of the Congo craton, comprises Neoproterozoic metasediments deposited in a passive margin environment and were metamorphosed under high P conditions at 616 Ma. An alkaline magmatism [17,18] was also recognized in association with these Neoproterozoic units; (2) the northern domain consists of subordinate 830 Ma-old metavolcanic rocks of tholeiitic and alkaline affinities associated with metasediments known as the Poli series. Widespread 630-660 Ma-old calc-alkaline granitoids, presently orthogneissified, result from a major episode of crustal accretion; (3) the central domain, which contains the present study area, is positioned between the Sanaga fault and the Betare-Oya shear zone (BOSZ) to the south and the Tibati-Banyo fault to the north. These large NE-striking transcurrent faults, as well as the Adamaoua fault inside the central domain, are regarded as possible prolongations of the major shear zones of NE Brazil in a pre-drift Gondwana reconstruction [19-26]. The central domain consists of Archean to Paleoproterozoic high-grade gneisses intruded by widespread Neoproterozoic syntectonic plutonic rocks of high-K calc-alkaline affinities [11,12,16,27,28,29,30]. The hosting basement rocks were intensively reworked during a polyphase Pan-African  $D_1$ - $D_2$  deformation associated with amphibolite

facies metamorphism. Ngoura-Colomines area is located in eastern part of the central domain. Previous geological investigations [31] have recognized of orthogneiss and migmatite intruded by granitoids. These granitoids include syn- to post-tectonic granite and granodiorite [32] (Figure 4).

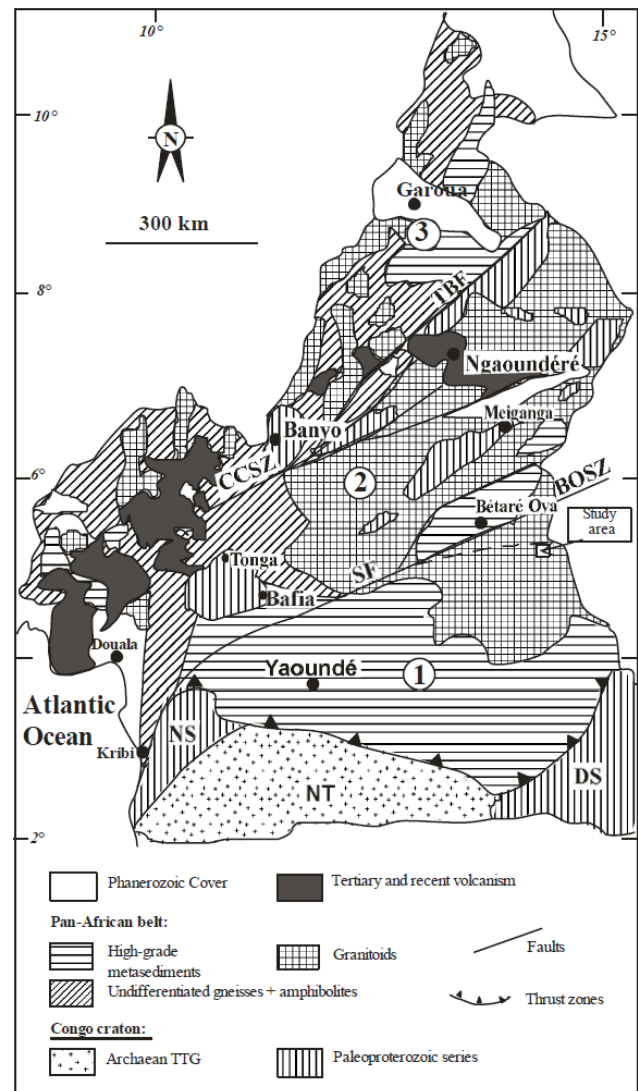


**Figure 3.** Geologic map of Cameroon [12] showing the location of the Ngoura-Colomines area and the main lithotectonic domains: (1) southern domain; (2) central domain; (3) northern domain; BOSZ: Bétaré-Oya Shear Zone; SF: Sanaga Fault; TBF: Tibati-Banyo Fault; NT: Ntem complex; DS: Dja Series; NS: Nyong Series

### 3. Material and Methods

#### 3.1. Types of Used Data

Various types of datum were used in this study. These data included: (i) Landsat-7 ETM+ images (Path 184 and Row 057) of December 24, 2003 (beginning of the dry season) and corresponding to Zone 33 of the map projection, Universal Transverse Mercator (UTM) which uses the geodetic reference system WGS 84; (ii) the SRTM satellite image covering the area of study; (iii) the geologic map of Batouri East at the 1/500 000 [31], and (iv) the topographic map of scale 1/200 000 covering the explored area. The choice of these images was based on their spectral characteristics and spatial resolution. The

main characteristics of the Landsat satellite images used in this study are presented in Table 1. The analysis of the

different resulting maps was made using ArcGIS 10, Erdas Imagine 2014, and Geomatica 2012 software

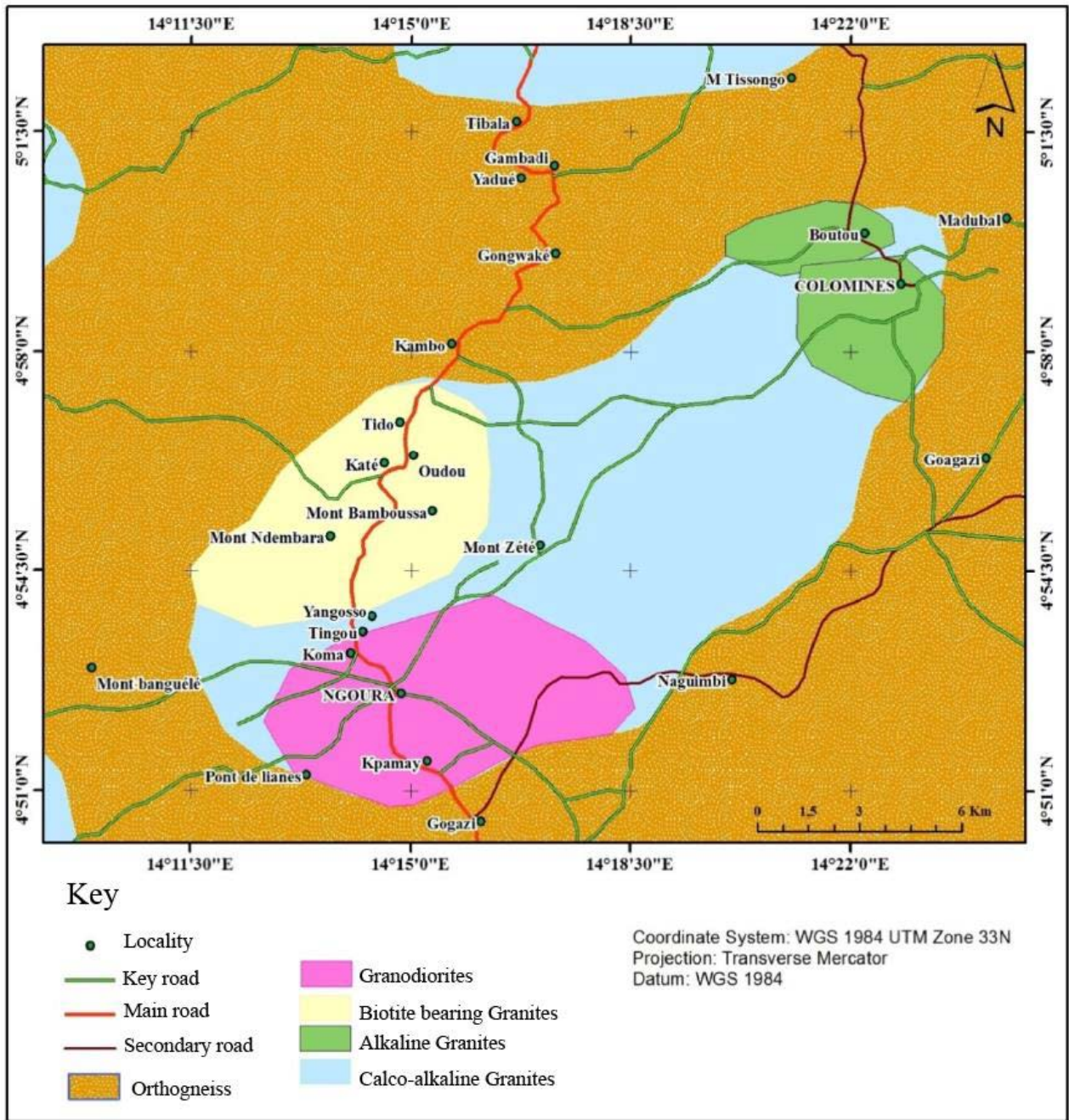


Figure 4. Geologic map of the studied area (modified from [31])

Table 1. Characteristics of the Landsat 7 ETM+ bands used in this study

Frequency bands of the ETM+ instrument	Spectral bands	Spatial resolution	Wavelength
Band 1	Blue (visible)	30 m	0.45 - 0.5 μm
Band 2	Green (visible)	30 m	0.52 - 0.6 μm
Band 3	Red (visible)	30 m	0.63 - 0.69 μm
Band 4	Near IR	30 m	0.75 - 0.9 μm
Band 5	Medium IR	30 m	1.5 - 1.7 μm
Band 6/1	Thermal IR / distant	60 m	10.4 - 12.5 μm
Band 6/2		120 m	
Band 7	Medium IR	30 m	2.08 - 2.35 μm
Band 8	Panchromatic (Green-Red-IR)	15 m	520 - 900 nm

### 3.2. Treatment Methods of Satellite Images

There are a wide variety of techniques for the improvement of the satellite images. The choice of a particular technology depends on its application, the available data, the experience and preferences of the image analyst. Different types of treatments were carried out. The aim of the image processing was to obtain a particular spectral signature for the lithology and to make the lineament easily detectable. This approach requires a pre-treatment which assumes a good knowledge of the sensor and of the conditions of acquisition. It is not subject to a particular thematic application and allows the development of an image from a raw signal and the improvement of the said image. The pre-treatment operations consisted in this case in radiometric and geometric corrections, so as to remedy error images and the different distortions caused by the movement of the platform, generally caused by atmospheric disturbances.

#### 3.2.1. Improvement or Enhancement of the Contrast

An enhancement operator aims to replace the central pixel by the sum of the differences with its neighbors. Images thus corrected have been processed with the aim of increasing their visual perception (improvement of quality to make them more expressive) which leads to a better visualization of discontinuities. To do this, four main techniques were used: (i) the Principal Component

Analysis (PCA); (ii) coloured composition; (iii) the combination of bands and, (iv) spatial filtering.

#### -The Principal Component Analysis (PCA)

The principal component analysis (PCA) is part of the group of multidimensional descriptive methods called Factorial methods. To compress the redundant data of multi-band images and find a combination of the most discriminatory colorful composition, PCA proposes from a rectangular array of data containing values of  $p$ , quantitative variable for  $n$  units (also called individuals), geometric representations of these units and these variables [33]. The raw ETM+ band are strongly correlated as shown in Table 2. The correlation matrix reflects the strong redundancy of the information contained in the Landsat-7 ETM+ images. It is therefore correct to carry out a principal component analysis in order to overcome the redundancy and to improve the contrast of the image. This technique also reduces the number of bands to be treated by compressing the information according to a hierarchy. Six ETM+ channels (1, 2, 3, 4, 5 and 7) with the same resolution (30 m) were retained for the PCA techniques. The result of the two first components (the neo-channels ACP1 and ACP2) represents respectively 70.6 and 13.2 % of the information contained in the original multi-spectral image with nine bands. The obtained transformed images contain the maximum information and were thus combined through a colorful composition.

Table 2. Correlation matrix of raw Landsat ETM+ bands

	ETM1	ETM2	ETM3	ETM4	ETM5	ETM7
ETM1	1.000000	0.738563	0.733769	0.005681	0.484322	0.639578
ETM2	0.738563	1.000000	0.839243	0.304762	0.724692	0.757614
ETM3	0.733769	0.839243	1.000000	0.072603	0.758965	0.890240
ETM4	0.005681	0.304762	0.072603	1.000000	0.549949	0.168209
ETM5	0.484322	0.724692	0.758965	0.549949	1.000000	0.874637
ETM7	0.639578	0.757614	0.890240	0.168209	0.874637	1.000000

#### - Colored composition

This technique consists in transforming the gray level pictures into colored three bands images by assigning one of the primary colors: red (R), green (G) and blue (B). In order to optimize the visual analysis and to adapt the variations of tones to the human visual system, the colorful compositions were applied to the ETM+ Landsat-7 image from the near infrared (NIR) and medium infrared (MIR1 and MIR2) bands respectively (Figure 5). In fact, each of these bands integrates additional information that could reveal the structure of the soil. This property allows the clearly discrimination between geologic features and the vegetation, thus facilitating the visual distinction of the lineament.

#### - Combination of bands

The combination of bands is an arithmetic operation (addition, subtraction, and division) applied on the bands. According to Kouame [34], TM7-TM4/TM7+TM4 band reports allows the visualization of the lineaments related to the hydrographic network, while TM6-TM7/TM6+TM7 bands helped to highlight the regional lineaments, e.g, the large-scale structures and the large fracture zones of the bedrock [35]. These fractures would either be faulted

zones or shear zones. This second report, which implies the use of the spectral band of the thermal/distant IR, has been possible only after the re-sampling of the TM6 band according to the same spatial resolution as the other bands. The application of the technique of bands combination is an asset for the structural mapping of the Ngoura-Colomines are due to the fact that the hydrographic network is dependent to the tectonics [32].

#### - Spatial filtering

The technique of spatial filtering of the image consists of the recalculation of the value of each pixel by analyzing the surrounding radiometry. The aim of this method is the increasing of the image's contrast. A linear filter convolutes the radiometry of the image by convolution windows (small square matrix centered on the current pixel) whose coefficients determine the effect of the filtering [36]. In this study the convolution is applied on an image  $I(x, y)$  with a function  $f(x, y)$  called impulse response (or convolution operator) of the filter. In a general case, the filtered image is given by:

$$I_f(x, y) = (f \times I)(x, y) \\ = \int_{-\infty}^{+\infty} \int_{-\infty}^{+\infty} f(x', y') I(x - x', y - y') dx' dy'$$

In a specific case and to take the simplified example of a square image, the areas of  $I$  and  $f$  have end points. The domain of  $I$  is  $[-N/2, +N/2]^2$  if  $N$  refers to the size of the image and the domain of  $f$  is  $[-K/2, +K/2]^2$  with  $K \leq N$  necessarily. The convolution is then written:

$$I_f(x, y) = (f \times I)(x, y) = \sum_{i'=-k/2}^{i'+k/2} \sum_{j'=-k/2}^{j'+k/2} f(i-i', j-j')I(i', j')$$

We can notice that the linear filtering simply consists in replacing each gray level by a linear combination of the gray levels of the neighboring points. The filters used here are the directional filters which are applied in four (4) main directions: N-S, E-W, NE-SW, SE-NW. Table 3 gives an example of convolution matrixes for the directional filters of Sobel used in this study. Sobel's algorithm is an operator used in image processing for the detection of contours.

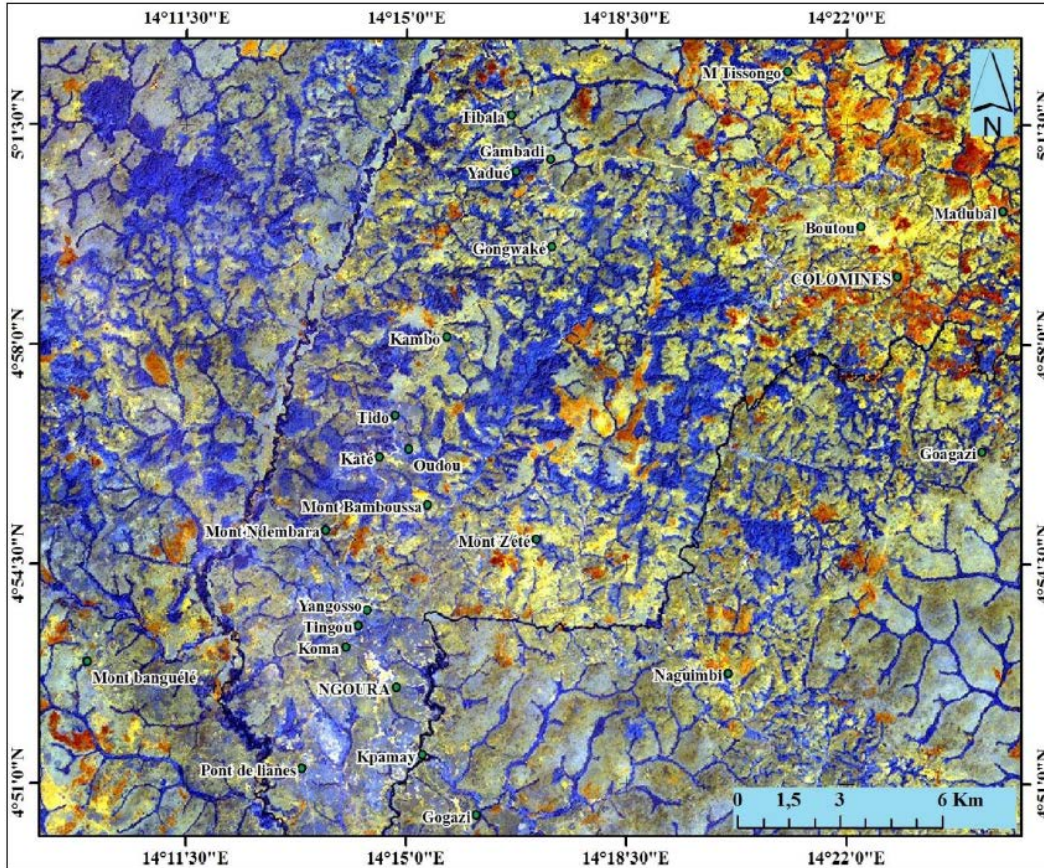


Figure 5. RGB 754 coloured composition image of the area of study area

Table 3. Convolution matrixes of the Sobel 7 x 7 filter and the gradient of Yésou et al. [37]

<table border="1"> <tr><td>1</td><td>1</td><td>1</td><td>2</td><td>1</td><td>1</td><td>1</td></tr> <tr><td>1</td><td>1</td><td>2</td><td>3</td><td>2</td><td>1</td><td>1</td></tr> <tr><td>1</td><td>2</td><td>3</td><td>4</td><td>3</td><td>2</td><td>1</td></tr> <tr><td>0</td><td>0</td><td>0</td><td>0</td><td>0</td><td>0</td><td>0</td></tr> <tr><td>-1</td><td>-2</td><td>-3</td><td>-4</td><td>-3</td><td>-2</td><td>-1</td></tr> <tr><td>-1</td><td>-1</td><td>-2</td><td>-3</td><td>-2</td><td>-1</td><td>-1</td></tr> <tr><td>-1</td><td>-1</td><td>-1</td><td>-2</td><td>-1</td><td>-1</td><td>-1</td></tr> </table> <p>Sobel N-S</p>	1	1	1	2	1	1	1	1	1	2	3	2	1	1	1	2	3	4	3	2	1	0	0	0	0	0	0	0	-1	-2	-3	-4	-3	-2	-1	-1	-1	-2	-3	-2	-1	-1	-1	-1	-1	-2	-1	-1	-1	<table border="1"> <tr><td>-1</td><td>-1</td><td>-1</td><td>0</td><td>1</td><td>1</td><td>1</td></tr> <tr><td>-1</td><td>-1</td><td>-2</td><td>0</td><td>2</td><td>1</td><td>1</td></tr> <tr><td>-1</td><td>-2</td><td>-3</td><td>0</td><td>3</td><td>2</td><td>1</td></tr> <tr><td>-2</td><td>-3</td><td>-4</td><td>0</td><td>4</td><td>3</td><td>2</td></tr> <tr><td>-1</td><td>-2</td><td>-3</td><td>0</td><td>3</td><td>2</td><td>1</td></tr> <tr><td>-1</td><td>-1</td><td>-2</td><td>0</td><td>2</td><td>1</td><td>1</td></tr> <tr><td>-1</td><td>-1</td><td>-1</td><td>0</td><td>1</td><td>1</td><td>1</td></tr> </table> <p>Sobel E-W</p>	-1	-1	-1	0	1	1	1	-1	-1	-2	0	2	1	1	-1	-2	-3	0	3	2	1	-2	-3	-4	0	4	3	2	-1	-2	-3	0	3	2	1	-1	-1	-2	0	2	1	1	-1	-1	-1	0	1	1	1	<table border="1"> <tr><td>0</td><td>1</td><td>1</td><td>1</td><td>1</td><td>1</td><td>2</td></tr> <tr><td>-1</td><td>0</td><td>2</td><td>2</td><td>2</td><td>3</td><td>1</td></tr> <tr><td>-1</td><td>-2</td><td>0</td><td>3</td><td>4</td><td>2</td><td>1</td></tr> <tr><td>-1</td><td>-2</td><td>-3</td><td>0</td><td>3</td><td>2</td><td>1</td></tr> <tr><td>-1</td><td>-2</td><td>-4</td><td>-3</td><td>0</td><td>2</td><td>1</td></tr> <tr><td>-1</td><td>-3</td><td>-2</td><td>-2</td><td>-2</td><td>0</td><td>1</td></tr> <tr><td>-2</td><td>-1</td><td>-1</td><td>-1</td><td>-1</td><td>-1</td><td>0</td></tr> </table> <p>Sobel NE-SW</p>	0	1	1	1	1	1	2	-1	0	2	2	2	3	1	-1	-2	0	3	4	2	1	-1	-2	-3	0	3	2	1	-1	-2	-4	-3	0	2	1	-1	-3	-2	-2	-2	0	1	-2	-1	-1	-1	-1	-1	0
1	1	1	2	1	1	1																																																																																																																																															
1	1	2	3	2	1	1																																																																																																																																															
1	2	3	4	3	2	1																																																																																																																																															
0	0	0	0	0	0	0																																																																																																																																															
-1	-2	-3	-4	-3	-2	-1																																																																																																																																															
-1	-1	-2	-3	-2	-1	-1																																																																																																																																															
-1	-1	-1	-2	-1	-1	-1																																																																																																																																															
-1	-1	-1	0	1	1	1																																																																																																																																															
-1	-1	-2	0	2	1	1																																																																																																																																															
-1	-2	-3	0	3	2	1																																																																																																																																															
-2	-3	-4	0	4	3	2																																																																																																																																															
-1	-2	-3	0	3	2	1																																																																																																																																															
-1	-1	-2	0	2	1	1																																																																																																																																															
-1	-1	-1	0	1	1	1																																																																																																																																															
0	1	1	1	1	1	2																																																																																																																																															
-1	0	2	2	2	3	1																																																																																																																																															
-1	-2	0	3	4	2	1																																																																																																																																															
-1	-2	-3	0	3	2	1																																																																																																																																															
-1	-2	-4	-3	0	2	1																																																																																																																																															
-1	-3	-2	-2	-2	0	1																																																																																																																																															
-2	-1	-1	-1	-1	-1	0																																																																																																																																															
<table border="1"> <tr><td>2</td><td>1</td><td>1</td><td>1</td><td>1</td><td>1</td><td>0</td></tr> <tr><td>1</td><td>3</td><td>2</td><td>2</td><td>2</td><td>0</td><td>-1</td></tr> <tr><td>1</td><td>2</td><td>4</td><td>3</td><td>0</td><td>-2</td><td>-1</td></tr> <tr><td>1</td><td>2</td><td>3</td><td>0</td><td>-3</td><td>-2</td><td>-1</td></tr> <tr><td>1</td><td>2</td><td>0</td><td>-3</td><td>-4</td><td>-2</td><td>-1</td></tr> <tr><td>1</td><td>0</td><td>-2</td><td>-2</td><td>-2</td><td>-3</td><td>-1</td></tr> <tr><td>0</td><td>-1</td><td>-1</td><td>-1</td><td>-1</td><td>-1</td><td>-2</td></tr> </table> <p>Sobel NW-SE</p>	2	1	1	1	1	1	0	1	3	2	2	2	0	-1	1	2	4	3	0	-2	-1	1	2	3	0	-3	-2	-1	1	2	0	-3	-4	-2	-1	1	0	-2	-2	-2	-3	-1	0	-1	-1	-1	-1	-1	-2	<table border="1"> <tr><td>1</td><td>1</td><td>1</td><td>1</td><td>1</td><td>1</td><td>1</td></tr> <tr><td>1</td><td>1</td><td>1</td><td>1</td><td>1</td><td>1</td><td>1</td></tr> <tr><td>1</td><td>1</td><td>1</td><td>1</td><td>1</td><td>1</td><td>1</td></tr> <tr><td>0</td><td>0</td><td>0</td><td>0</td><td>0</td><td>0</td><td>0</td></tr> <tr><td>-1</td><td>-1</td><td>-1</td><td>-1</td><td>-1</td><td>-1</td><td>-1</td></tr> <tr><td>-1</td><td>-1</td><td>-1</td><td>-1</td><td>-1</td><td>-1</td><td>-1</td></tr> <tr><td>-1</td><td>-1</td><td>-1</td><td>-1</td><td>-1</td><td>-1</td><td>-1</td></tr> </table> <p>Yésou et al. (1993)[37]</p>	1	1	1	1	1	1	1	1	1	1	1	1	1	1	1	1	1	1	1	1	1	0	0	0	0	0	0	0	-1	-1	-1	-1	-1	-1	-1	-1	-1	-1	-1	-1	-1	-1	-1	-1	-1	-1	-1	-1	-1																																																		
2	1	1	1	1	1	0																																																																																																																																															
1	3	2	2	2	0	-1																																																																																																																																															
1	2	4	3	0	-2	-1																																																																																																																																															
1	2	3	0	-3	-2	-1																																																																																																																																															
1	2	0	-3	-4	-2	-1																																																																																																																																															
1	0	-2	-2	-2	-3	-1																																																																																																																																															
0	-1	-1	-1	-1	-1	-2																																																																																																																																															
1	1	1	1	1	1	1																																																																																																																																															
1	1	1	1	1	1	1																																																																																																																																															
1	1	1	1	1	1	1																																																																																																																																															
0	0	0	0	0	0	0																																																																																																																																															
-1	-1	-1	-1	-1	-1	-1																																																																																																																																															
-1	-1	-1	-1	-1	-1	-1																																																																																																																																															
-1	-1	-1	-1	-1	-1	-1																																																																																																																																															

In practice, the operator calculates the gradient of the intensity of each pixel. This indicates the direction of the greatest variation from light to dark, as well as the rate of change in this direction. We know then the points of

sudden change in brightness, corresponding probably to the edges, as well as the orientation of these edges. The operator uses convolution matrix. The matrix (in the present case of size  $7 \times 7$ ) undergoes a convolution with

the image to calculate approximations from horizontal and vertical derivatives. These filters with respect to sliding 7 x 7 windows have been applied to neo-PCA channels to accentuate the lithological and structural discontinuities, and facilitate the discrimination of the lineament. After the filtering of images following the mentioned directions, the next step was in the manual and automatic extraction of lineaments.

**3.2.2. Extraction of the Lineament by Photo-Interpretation**

Based on the available data and with the help of field observations, the automatic and manual extraction of lineaments has been undertaken in the framework of this study. Nevertheless, it has been capital to design a

geographic information system (GIS) database of the entire anthropic features (road network, electric cables, forest delimitation and cultivated areas, etc.) listed in the explored area. The superimposition of these features on the final rendering allows us to eliminate all unwanted features because only lineaments of tectonic origin are the scope of this study. Manual extraction consisted in digitalizing of all linear structures observed on the transformed, enhanced and filtered satellite image. The automatic extraction of the second family of major lineaments was made using the satellite image processing software Geomatica 2012. The final structural map is obtained after the validation of the automatic extracted lineaments by comparison with those observed in the field.

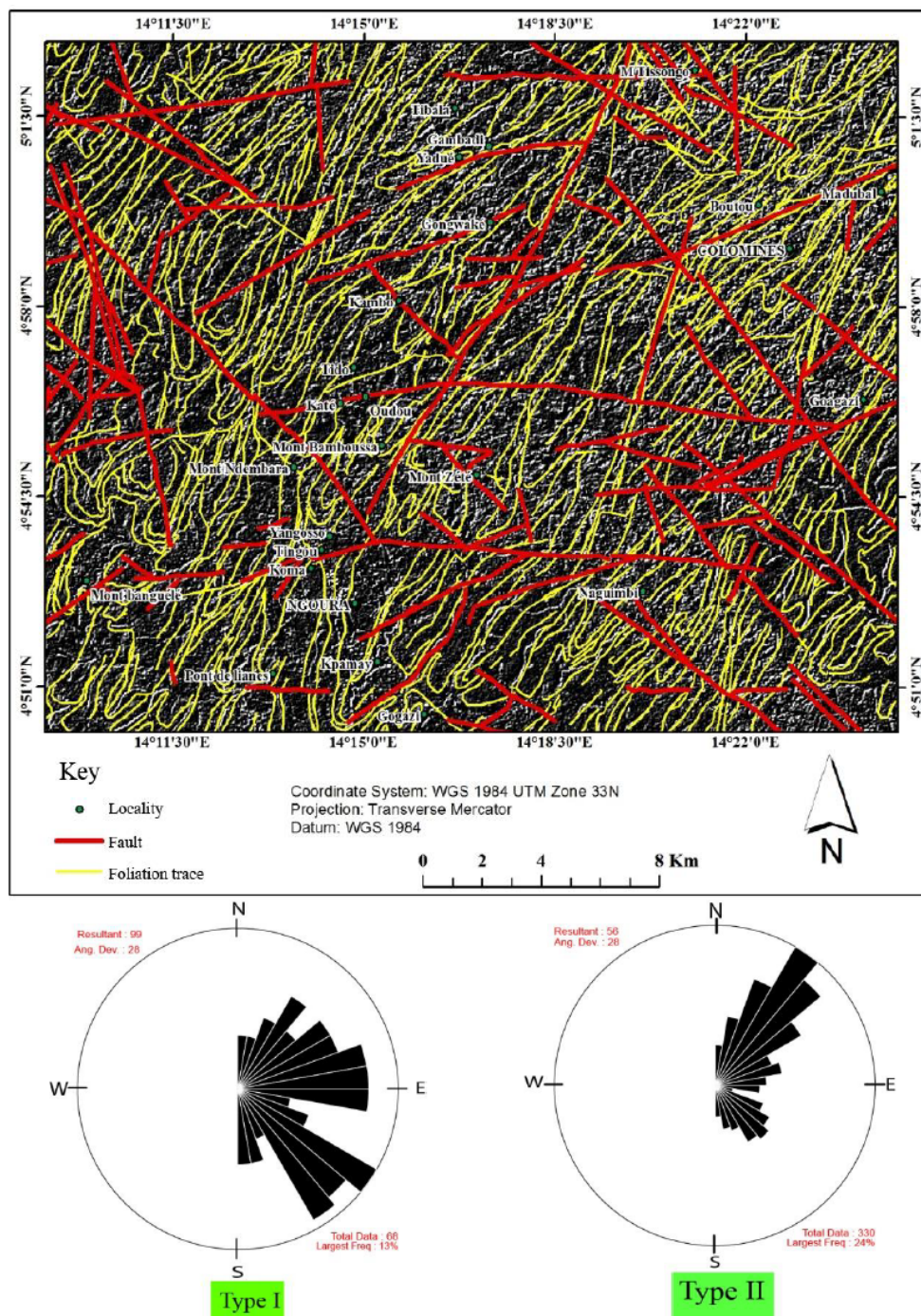


**Figure 6.** Major tectonic accidents depicted by the Sobel filtering and the Yésou et al. [37] gradient applied to the PCA 1 image and associated directional rosette

## 4. Results and Discussion

### 4.1. Structural Mapping and characteristics of the Lineament Frame

After transformation, enhancement and filtering of the images, both automatic extraction and visual interpretation enabled us to highlight the tectonic lineaments and to notice their locally curved junctions. With the purpose of studying the geometry of the lineament network and identifying the dominant directions, a statistical analysis was carried out. This analysis identified 654 linear elements. These lineaments show rectilinear trajectories sporadically relayed by curves. Two main types of lineaments have been distinguished. The first type or type-I corresponds to large-scale or regional structures. It is characterized by a more accentuated tracing, a mapping continuity and a sparser spatial density and represents

about 15% of the frame while the second type (type-II) represents approximately 85% and is made up of curved portions. Figure 6 presents the results of the directional filtering on which type-I regional lineaments have been manually digitalized, while the lineaments with curved portions (type-II) were automatically generated. Also, type-I linear structures induce the offset of the type II lineaments at their contact and thus represent fractures in the study area. Type-II linear structures, due to their penetrative character, correspond to the foliation trace. This interpretation is confirmed by field data which have revealed foliation surfaces with NE-SW-trends. The rose diagrams associated to the two lineament types are also presented in the Figure 6. These directional diagrams show two main directions (NE-SW and NW-SE) for type-I lineaments and a dominant NE-SW-trends and secondary N-S and E-W-trends for foliation trace (type-II linear structures).

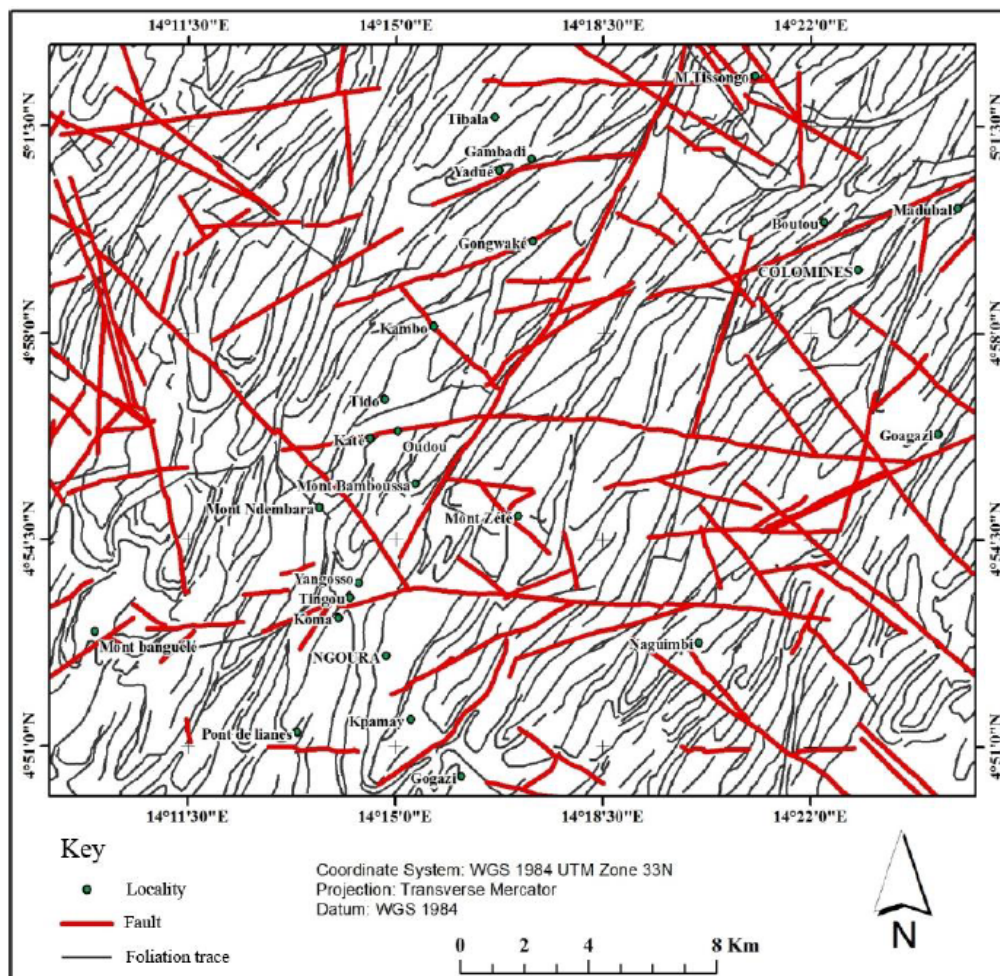


Figure 7. Structural map of the Ngoura-colomines area obtained from the analysis of Landsat 7 ETM+ images

Figure 7 presents the structural map of the study area obtained from the analysis of both satellite images and the topographic map. This map shows the general configuration of the principal strike-slip fault and associated satellite faults, and the predominant NE-SW direction of foliation trajectories in the study area. Figure 8 is the detailed geologic map of the Ngoura-Colomines area obtained from the combination of the structural map layer and the reconnaissance lithological map layer of Gazel and Gerard [31].

### 4.2. Tectonic Architecture and Evidence for the Riedel Fractures System

The structural map (Figure 7) has been superimposed to the hydrographic network in order to obtain the morphostructural map of the study area (Figure 9). On this map, it is important to notice that the foliation trajectories are shifted away by fractures. This is indicative of the lateness character of the fractures with respect to the tectonic episodes.

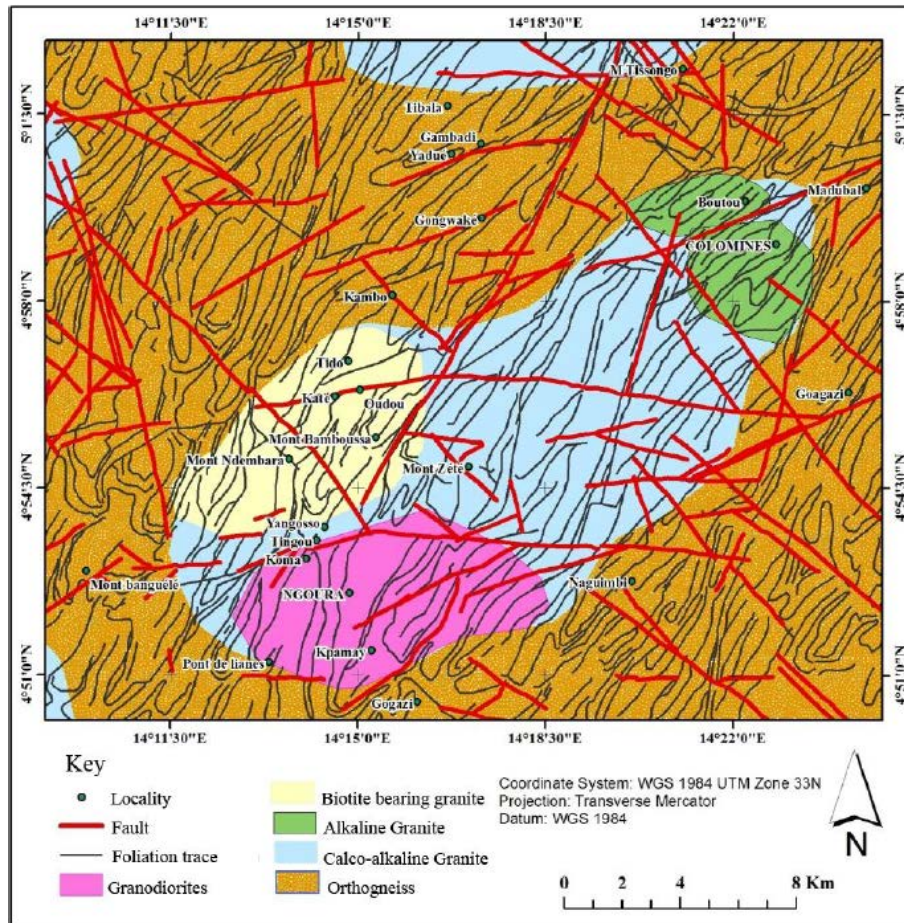


Figure 8. Geologic map of the Ngoura-Colomines area obtained from the combined field-based and remote sensing methods

In addition, five (05) major families of fractures have been distinguished: (i) the first one corresponds to a network of dextral shear planes with ENE-WSW direction; satellite faults of this network formed the Riedel fractures system composed of: (ii) P' fractures with NNE-SSW-

trend; (iii) R' fractures oriented NW-SE; (iv) R fractures trending E-W; and (v) P fractures with NE-SW direction. At the map scale, the foliation trajectories show a mega folding structure resulting from WNW-ESE to NW-SE shortening.

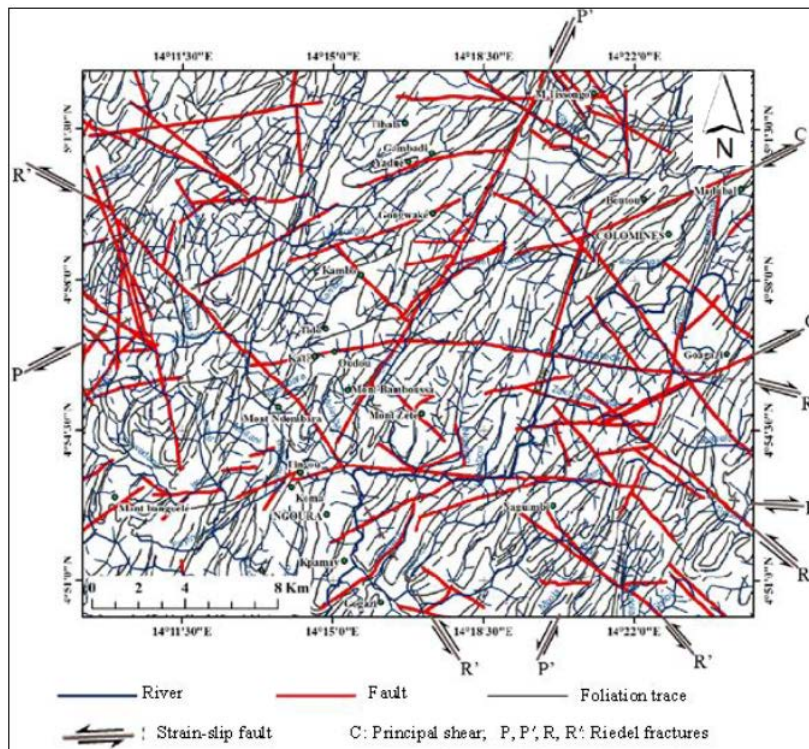


Figure 9. Morphostructural map of Ngoura-Colomines area showing the principal shear zone (C) and the Riedel faults system (P, P', R and R')

The distribution frequency of the tectonic lineaments is shown in Figure 10, where the lineaments are grouped in classes according to their length. At the regional scale, the main strike-slip faults identified in this study have the same direction with both the Sanaga fault [38] and the Bétaré-Oya fault [25], pointing to the prolongation of these regional structures in the Ngoura-Colomines area.

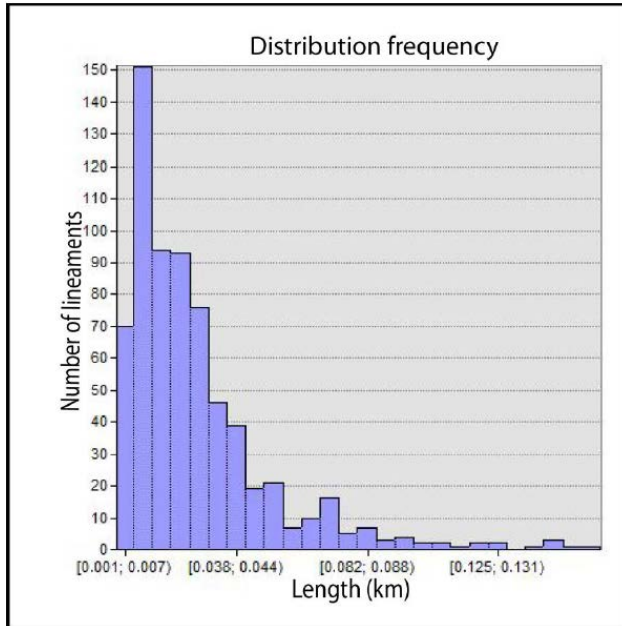


Figure 10. Histogram showing the distribution frequency of lineaments

### 4.3. Relationship between Field Data and Satellite Imagery Data

The Ngoura-Colomines area is composed mainly of syn- to post-tectonic granitoids. Field investigations have consisted of exploring the outcrops, identifying and measuring the geological structures. Geometric analysis of these structures has revealed three main deformational phases.

- The first phase ( $D_1$ ) is associated with the development of  $S_1$  mylonitic foliation and  $B_1$  boudins (Figure 11A).  $S_1$  foliation is outlined by composition banding (Figure 11B) and by the preferred orientation of minerals (Figure 11A), while the  $B_1$  boudins are developed on both the mafic and the quartzofeldspathic layers (Figure 11B), and can be attributed to multilayer boudins of Ghosh and Sengupta [39].

- The second deformation phase ( $D_2$ ) is marked by boudinated aplitic and pegmatite dykes crosscutting the  $S_m$  foliation, and the conjugated shear structures with sinistral shear movement (Figure 11C and Figure 11D).

- The last tectonic phase ( $D_3$ ) is mainly brittle and marked by fractures including dyke and faults, which affect the  $D_1$  and  $D_2$  structures (Figure 11E). Their directions vary from N045E to N115E, similar to Type-II lineament depicted from Landsat image processing.

Overall, the geological structures obtained from the image processing correspond to the ductile-brittle structures such as shear zone and faults. These structures constitute pathway for both mineralizing fluids and ground water.

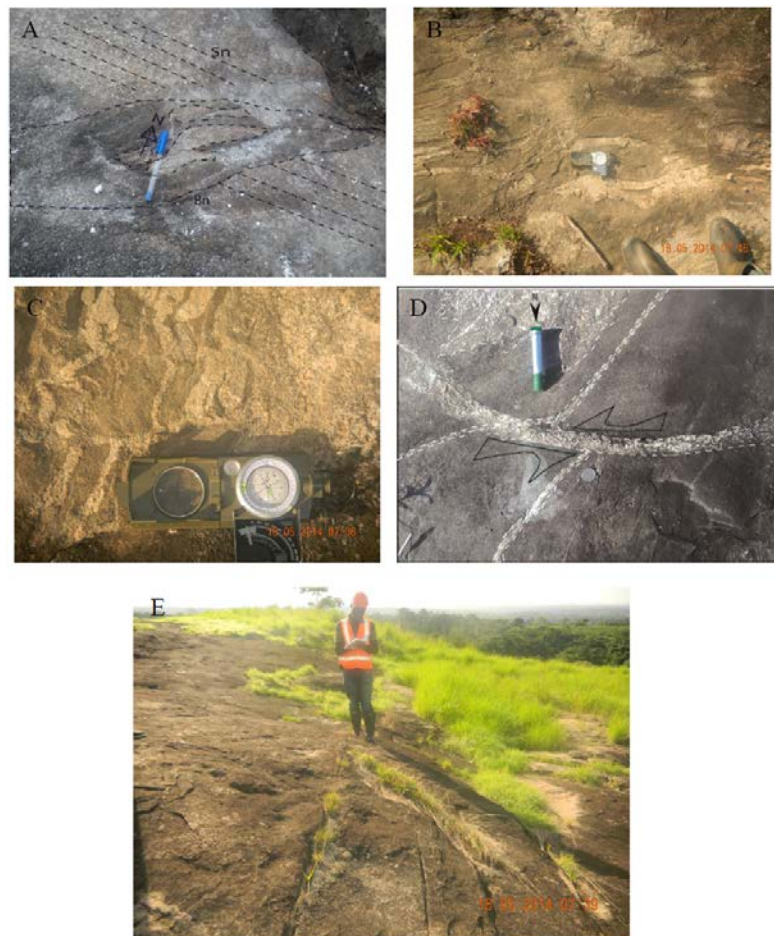


Figure 11. Structures identified during the field (a) Boudin of amphibolite encased in mylonitic foliation (b) Lithologic banding with intrafolial boudinage (c) Conjugated shearing, note the chocolate bar structure (d) Sinistral shearing structures (e) Brittle structures

## 5. Conclusion

The use of Landsat-7 ETM+ images in the Ngoura-Colomines area has allowed the development a new methodology for the mapping of major regional tectonic accidents. The obtained lithotectonic map of Ngoura-Colomines is the result of several treatments performed on the satellite images and validated with the field survey. The combination of field-based mapping and remote sensing methods are useful tool for the mapping of regional geological structures. The present study has shown that the satellite data is very useful in various aspects of geological, geomorphological and lineament mapping studies. The proposed method allows the detail lineament mapping in rainforest area and could be applied in other areas elsewhere. Since several gold artisanal mines exist in Ngoura-Colomines area, the new mapping approach could constituted an important guide for the identification of the structures that control the gold mineralisation in the area.

## Acknowledgements

The data presented here form a part of the first author's Ph.D thesis supervised by S. Ganno and J.P. Nzenti at the University of Yaoundé I, Cameroon. We gratefully acknowledge the anonymous reviewers for their critical and constructive comments of the manuscript. This is the contribution to ICGP-Y 646 project.

## References

- [1] Parsons, A.J., Yearley, R.J. An analysis of geologic lineaments seen on Landsat MSS imagery. *International Journal of Remote Sensing*, 7(12), 1773-1782, 1986.
- [2] Ozer, A., Marion, J.M., Roland, C., Tréfois, P. Signification des linéaments sur une image S.P.O.T. dans la région liégeoise. *Bulletin de la Société Belge de Géologie*, 97(2), 153-172, 1988.
- [3] Metang, V., Nkoumbou, C., Tchakounté, N.J., Njopwouo, D. Application of remote sensing for the mapping of geological structures in rainforest area: a case study at the Matomb-Makak area, Center-South Cameroon. *Journal of Geosciences and Geomatics*, 2(5), 196-207, 2014.
- [4] Koffi Y., T. Extraction de linéaments structuraux à partir d'images satellitaires, et estimation des biais induits en milieu de socle. *Revue de télédétection*, 161-178, 2011.
- [5] Scavic, J.Y. Utilisation de la télédétection dans les sciences de la terre. *Manuels et Méthodes, Éditions du BRGM, Orléans, France*, 159 p., 1983.
- [6] Faillat, J.P. Hétérogénéité et effet d'échelle dans les aquifères fissurés. Approches par pompages d'essais sur station expérimentale (Afrique de l'Ouest). *BRGM, Hydrogéologie*, 1, 65-76, 1986.
- [7] Biemi J. Contribution à l'étude géologique, hydrogéologique et par télédétection des bassins versants subsabéliens du socle précambrien d'Afrique de l'ouest: hydrostructurale, hydrodynamique, hydrochimie et isotopie des aquifères discontinus des sillons et aires granitiques de la haute Marahoué (Côte d'Ivoire). *Thèse de Doctorat d'état, Université Nationale de Côte d'Ivoire*, 479 p., 1992.
- [8] Horton, R. Erosional development of streams and their drainage basins: hydrological approach to quantitative morphology. *Bulletin Geological Society of America, New York*, 56, 275-370, 1945.
- [9] Bessoles, B. Géologie de l'Afrique: le craton Ouest-africain. *Mémoire BRGM, France*, 88, 403p., 1977.
- [10] Akame, J.M., Mvondo Ondo, J., Assatse, T.W., Owona, S., Olinga, J.B, Messi, O.E.J, Ntomba, S. Apport des images landsat-7 ETM+ à l'étude structurale du socle archéen de Sangmélima (Sud-Cameroun). *Revue Française de Photogrammétrie et de Télédétection*, 206, 15-25, 2014.
- [11] Nzenti, J.P., Barbey, P., Bertrand, J.M., Macaudière, J. La Chaîne panafricaine au Cameroun: Cherchons suture et modèle. *15ème Réunion des Sciences de la Terre, Nancy, France, Société Géologique de France*, p. 99, 1994.
- [12] Nzenti, J.P., Abaga, B., Suh, C.E., Nzolang, C. Petrogenesis of peraluminous magmas from the Akum-Bamenda Massif, Pan-African Fold Belt, Cameroon. *International Geology Review*, 53(10), 1121-1149, 2011.
- [13] Ngotue, T., Nzenti, J.P., Barbey, P., Tchoua, F.M. The Ntui-Bétamba high-grade gneisses: a northward extension of the pan-African Yaoundé gneisses in Cameroon. *Journal of African Earth Sciences*, 31, 369-381, 2000.
- [14] Ngako, V., Affaton, P., Nnange, J.M., Njanko, T. Panafrican tectonic evolution in central and Southern Cameroon: transpression and transtension during sinistral shear movement. *Journal of African Earth Sciences*, 36, 207-214, 2003.
- [15] Mvondo, H., Owona, S., Mvondo, J., Essono, J. Tectonic evolution of the Yaoundé segment of the Neoproterozoic Central African Orogenic Belt in southern Cameroon. *Canadian Journal of Earth Sciences*, 44, 433-444, 2007.
- [16] Tanko Njiosseu, E.L., Nzenti, J.P., Njanko, T., Kapajika, B., Nedelec, A. New U/Pb zircon âges from Tonga (Cameroon): Coexisting Eburnean-Transamazonian (2.1 Ga) and Pan-African (0.6 Ga) imprints. *Compte Rendu Géosciences*, 337, 551-562, 2005.
- [17] Nzenti, J.P. L'Adamaoua panafricain (région de Banyo) : une zone clé pour un modèle de la chaîne panafricaine nord-équatoriale au Cameroun. *Thèse Doctorat d'État, Université Cheikh Anta Diop - Université de Nancy I*, 176 p., 1998.
- [18] Ngotue, T., Ganno, S., Nzenti, J.P., Schulz, B., Tchaptchet, T.D., Suh, C.E. Geochemistry and geochronology of Peraluminous high-K granitic leucosomes of Yaoundé series (Cameroon): evidence for a unique Pan-African magmatism and melting event in north equatorial fold belt. *International Journal of Geosciences*, 3, 525-548, 2012.
- [19] Castaing, C., Triboulet, C., Feybesse, J.L., and Chèvremont, P. Tectonometamorphic Evolution of Ghana, Togo, Benin in the light of the Pan-African/Braziliano orogeny. *Tectonophysics*, 218, 323-347, 1994.
- [20] Trompette, R. Geology of western Gondwana (2000 - 500Ma). Pan-African-Braziliano aggregation of South America and Africa. *A.A. Balkema, Rotterdam, the Netherlands*, 350p., 1994.
- [21] Brito Neves, B.D., Van Schmus, W.R., Fetter, A. North-West Africa North-Eastern Brazil. Major tectonic links and correlation problems. *Journal of African Earth Sciences*, 34, 275-273, 2002.
- [22] Cordani, U.G., D'Agrella-Filho, M.S., Brito-Neves, B.B., Trindade, R.I.F. Tearing up Rodinia: the Neoproterozoic palaeogeography of South American cratonic fragments. *Terra Nova*, 15, 350 - 359, 2003.
- [23] Njonfang, E., Ngako, V., Moreau, C., Affaton, P., Diot, H. Restraining bands in high temperature shear zones: The "Central Cameroon Shear Zone", Central Africa. *Journal of African Earth Science*, 52, 9-20, 2008
- [24] Ganno, S., Nzenti, J.P., Ngotué, T., Kankeu, B., Kouankap Nono, G.D. Polyphase deformation and evidence for transpressive tectonics in the Kimbi area, Northwestern Cameroon Pan-African Fold Belt. *Journal of Geology and Mining Research*, 4 (2), 001-015, 2010.
- [25] Kankeu, B., Nzenti, J.P., Greiling, R.O., Ganno, S., Ngotué, T., Basahak, J. & Hell, J.V. Application de la technique de l'Anisotropie de la Susceptibilité Magnétique (ASM) à l'identification des structures géologiques: le cisaillement panafricain de Bétaré Oya dans le district aurifère de l'Est Cameroun. *Annales de la Faculté des Sciences, Série Sciences de la Terre*, 38 (1), 17-30, 2010.
- [26] Silva Filho, A.F.D., Guimarães, I.P., Van Schmus, W.R., Armstrong, R.A., Rangel da Silva, J.M., Osako, L.S., Cocentino, L.M. SHRIMP U-Pb zircon geochronology and Nd signatures of supracrustal sequences and orthogneisses constrain the Neoproterozoic evolution of the Pernambuco-Alagoas domain, southern part of Borborema Province, NE Brazil. *International Journal of Earth Sciences*, 103, 2155-2190, 2014.
- [27] Nzenti, J.P., Kapajika, B., Wörner, G., Lubala, R.T. Synkinematic emplacement of granitoids in a Pan-African shear zone in Central Cameroon. *Journal of African Earth Science*, 45, 74-86, 2006.

- [28] Nzolang, C., Kagami, H., Nzenti, J.P., Holtz, F. Geochemistry and preliminary Sr-Nd isotopic data on the Neoproterozoic granitoids from the Bantoun area, west Cameroon: evidence for a derivation from a paleoproterozoic to Archean crust. *Polar Geosciences*, 16, 196-226, 2003.
- [29] Djouka-Fonkwe, M.L., Schulz, B., Schüssler, U., Tchouankoué, J.P., Nzolang, C. Geochemistry of the Bafoussam Pan-African I- and S-type granitoids in western Cameroon. *Journal of African Earth Science*, 50, 148-167, 2008.
- [30] Ganwa, A.A., Wolfgang, F., Wolfgang, S., Cosmas, K.S., Mvondo Ondo, J., Muharrem, S., Tchakounté, J.N. Zircon 207Pb/206Pb evaporation as of panafrican metasedimentary in the Kombé II area (Bafia Group, Cameroon). *Journal of African Earth Sciences*, 51, 77-88, 2008.
- [31] Gazel, J., Gerard, G. Carte géologique de reconnaissance du Cameroun au 1/500000, feuille de Batouri-Est avec notice explicative. *Mémoire Direction des Mines et de la Géologie, Yaoundé, Cameroun*, 43 p., 1954.
- [32] Takodjou Wambo, J.D. Étude pétro-structurale et potentialités aurifères du secteur Ngoura-Colomines (Nord-Est de Batouri). *Unpublished Master thesis, University of Yaoundé I*, 120 p., 2015.
- [33] Duby, C., Robin, S. Analyse en Composantes Principales. *Institut National Agronomique Paris – Grignon*, 54 p., 2006.
- [34] Kouame, F. Méthode de cartographie des discontinuités-images extraites d'images satellitales: exemple de la région semi-montagneuse à l'ouest de la Côte d'Ivoire. *Télétection*, 1, 139-156, 1999.
- [35] Savané, I. Contribution à l'étude géologique et hydrogéologique des aquifères discontinus du socle cristallin d'Odienné Nord-Ouest de la Côte d'Ivoire). Apports de la télédétection et d'un Système d'Information Hydrogéologique à Référence Spatiale. *Thèse de doctorat ès Sciences Naturelles, Université d'Abidjan-Côte d'Ivoire*, 386 p., 1997.
- [36] Polidori, L. Introduction à la télédétection spatiale. *Manuel de cours, École Supérieure des Géomètres Topographes, France*, 60 p., 2006.
- [37] Yesou, H., Saint-Jean, R., Pion, J.C., Besnus, R. Amélioration des données SPOT pour la cartographie structurale en milieu tropical. Exemple de la région des chapeaux de fer de Pagala (Togo). In J.M.M. Dubois et F. Blasco (eds). Outils micro-informatiques et télédétection de l'évolution des milieux. *Série Actualité Scientifique, Presses de l'Université du Québec/AUPELF, Sainte-Foy*, 492 p., 1993.
- [38] Dumont, J.F. Identification par télédétection de l'accident de la Sanaga (Cameroun). Sa position dans le contexte des grands accidents d'Afrique Centrale et de la limite nord du craton congolais. *Géodynamique*, 1, 13-19, 1986.
- [39] Ghosh, S.K., Sengupta, S. Progressive evolution of structures in a ductile shear zone. *Journal of Structural Geology*, 9, 277-288, 1987.